Daubechies Versus Biorthogonal Wavelets for Moving Object Detection in Traffic Monitoring Systems

Mohammed A. Salem, Nivin Ghamry, and Beate Meffert

Abstract

Moving object detection is a fundamental task for a variety of traffic applications. In this paper the Daubechies and biorthogonal wavelet families are exploited for extracting the relevant movement information in moving image sequences in a 3D wavelet-based segmentation algorithm. The proposed algorithm is applied for traffic monitoring systems. The objective and subjective experimental results obtained by applying both wavelet types are compared and interpreted in terms of the different wavelet properties and the characteristics of the image sequences. The comparisons show the superior performance of the symmetric biorthogonal wavelets in the presence of noisy images and changing lighting conditions when compared to the application of high order Daubechies wavelets. The algorithm is evaluated using simulated images in the Matlab environment.

Index Terms— 3D wavelet transform, Image segmentation, Biorthogonal wavelets, Daubechies wavelets, traffic monitoring systems.

1 Introduction

Image segmentation is essential in many advanced techniques of multi-dimensional signal processing and its applications. The goal of segmentation is to simplify and/or change the representation of an image to make it more meaningful and easier to analyze. It is typically used to locate objects and boundaries (lines, curves, etc.) in images. Some of the practical applications of image segmentation are: medical imaging, diagnosis, face- and fingerprint recognition, machine vision and automatic traffic controlling systems. Image segmentation for traffic monitoring systems means detection and extraction of the moving objects that take part in the updated current traffic situation. In other words, active objects in an image sequence are encoded while the background, which may have moving and non-moving parts, is excluded. The development of reliable and efficient segmentation algorithms which can meet the requirements of the subsequent tracking and interpretation tasks as well as the high-speed response for real time applications is still a challenging problem. The most widely used image segmentation method for traffic or even outdoor moving object monitoring is based on background subtraction [2, 9, 20]. The background is initially set as the first frame of the video sequence [18, 6] or it is modelled as a Gaussian Mixture Model (GMM) [20]. In both cases, the background model must be updated in order to deal with changing lighting conditions and movements of irrelevant objects. Another approach uses a threshold based on the notion that vehicles

are compact objects having a different intensity as their background [13]. A general problem of this approach is that it cannot avoid false detection of shadows or missed detection of vehicle parts with similar intensities as its environment. Binary and grey-scale morphological operators can be used to improve background-foreground segmentation results [19]. In [6] background estimation and application of an adaptively updated threshold are combined. Some other approaches use a model based detection [11]. It is based on edge detection as a first step followed by fitting a proposed model. In [15] an image segmentation and moving object extraction algorithm applying the 3D Haar wavelet transform is presented. In [17] it is compared with the 2D wavelet-based algorithm proposed by Töreyin et al. [18] to assess the validity of the algorithm. That comparison shows that the 3D wavelet-based algorithm is more reliable to detect objects entering the scene than the 2D wavelet-based algorithm. Due to the multiresolution analysis the segmentation is speeded up and the performance of the algorithms is improved.

The application of Daubechies and the biorthogonal wavelets for edge detection was considered in [14] and further compared with other conventional methods in [3]. In both works it was found that the short wavelets are capable of better edge detection than long wavelets but the results were not explained in terms of the wavelet features. In the present work Daubechies as well as biorthogonal wavelets are used in the 3D wavelet-based algorithm of [15]. Here, the focus is on studying the different features of the wavelets, namely the symmetry of the biorthogonal wavelets and the irregularity of the high order Daubechies wavelets. Their effects on the image segmentation and moving object detection are investigated by comparing the simulation results of both types. The aim of this comparison is to get a relation between the features of the wavelets, the characteristics of the input image sequence, and the segmentation results.

The organization of the paper is as follows: In Section 2 the theory of Daubechies and biorthogonal wavelets is briefly surveyed. The 3D wavelet transform is explained in Section 3. Section 4 describes the 3D wavelet based algorithm. Section 5 presents the test data sets and the results of simulations. Matlab is used to assess the efficiency of the algorithm for the different wavelets objectively and subjectively. Finally, summary and conclusion are given.

2 Wavelets Overview

In this section a brief review of the principles and the theory of the orthogonal and biorthogonal wavelets is given to emphasize the features of each method.

2.1 Daubechies Wavelets

Daubechies constructed the first wavelet family of scale functions that are orthogonal and have finite vanishing moments, i.e., compact support [7]. This property insures that the number of non-zero coefficients in the associated filter is finite. This is very useful for local analysis. The Haar wavelet shown in Fig. 1(a) is the basis of the simplest wavelet transform. It is also the only symmetric wavelet in the Daubechies family and the only one that has an explicit expression in discrete form. Haar wavelets are related to a mathematical operation called Haar transform, which serves as a prototype for all other wavelet transforms. Like all wavelet trans-

forms, the Haar transform decomposes a discrete signal into two subsignals of half its length. One subsignal is a running average or trend, the other subsignal is a running difference or fluctuation. The Haar wavelet transform has the advantages of being conceptually simple, fast and memory efficient, since it can be calculated in place without a temporary array. Furthermore, it is exactly reversible without the edge effects that are a problem of other wavelet transforms. On the other hand, the Haar transform has its limitations because of its discontinuity, which can be a problem for some applications, like compression and noise removal of audio signal processing.

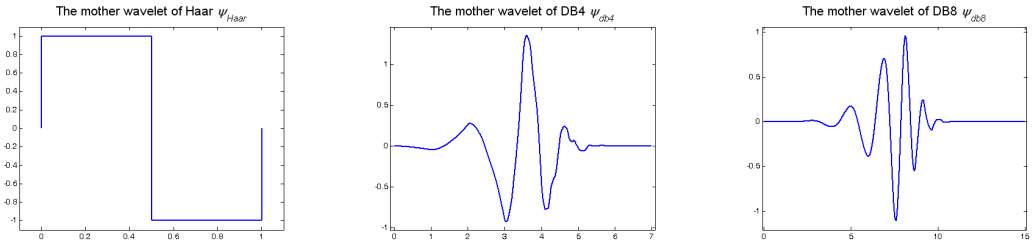

(a) (b) (c)

Figure 1: Mother wavelet functions of Haar, DB4, and DB8, respectively.

The Daubechies wavelet transforms are defined in the same way as the Haar wavelet transform by computing the running averages and differences via scalar products with scaling signals and wavelets. For higher order Daubechies wavelets ψ_{dbN}, N denotes the order of the wavelet and the number of the vanishing moments. The regularity increases with the order, as shown in Fig. 1. The support length is $2N-1$. The length of the associated filter is twice as the number of the vanishing moments, i.e., $2N$. The approximation and detail coefficients are of length $\mathsf{floor}(\frac{n-1}{2}) + N$, if n is the length of $(f(t))$ [12, 7]. This wavelet type has balanced frequency responses but non-linear phase responses. The regularity of the wavelets increases with the order. Figs. 1(b) and 1(c) show the wavelets $DB4$ and $DB8$. The wavelets with fewer vanishing moments give less smoothing and remove less details, but the wavelets with more vanishing moments produce distortions [10].

The analysis as proposed by Mallat [12] is done with some overlapping depending on the number of the vanishing moments N, due to the independence between the length of the wavelet function and the dyadic translation. The length of the associated filter is $2N$ and the translation k of the wavelet during the dyadic analysis is done in terms of the scale level $j \in \mathbb{Z}$ and not of the number of vanishing moments N of the wavelet, i.e., $k = 2^j b$, $b \in \mathbb{Z}$. For example, for the Haar wavelet ψ_{haar} there is no overlapping at all because the translation step is equal to the width of the wavelet. However, for the wavelet ψ_{db2} the overlapping is equal to 2 sample points. Generally, for a wavelet of order N at scale j the length of the associated filter is constant. Concerning the last discussion the detection of an event by higher order wavelets takes longer than that by lower order. Fig. 2 shows a 1D signal that has three main events. The first event appears in the beginning of the signal in the form of a zigzag line, the second one consists of three sharp edges, and the last event is a wide edge with a slow transition. The detail coefficients of two levels of analysis show that ψ_{haar} has the ability to localize the event even in higher levels.

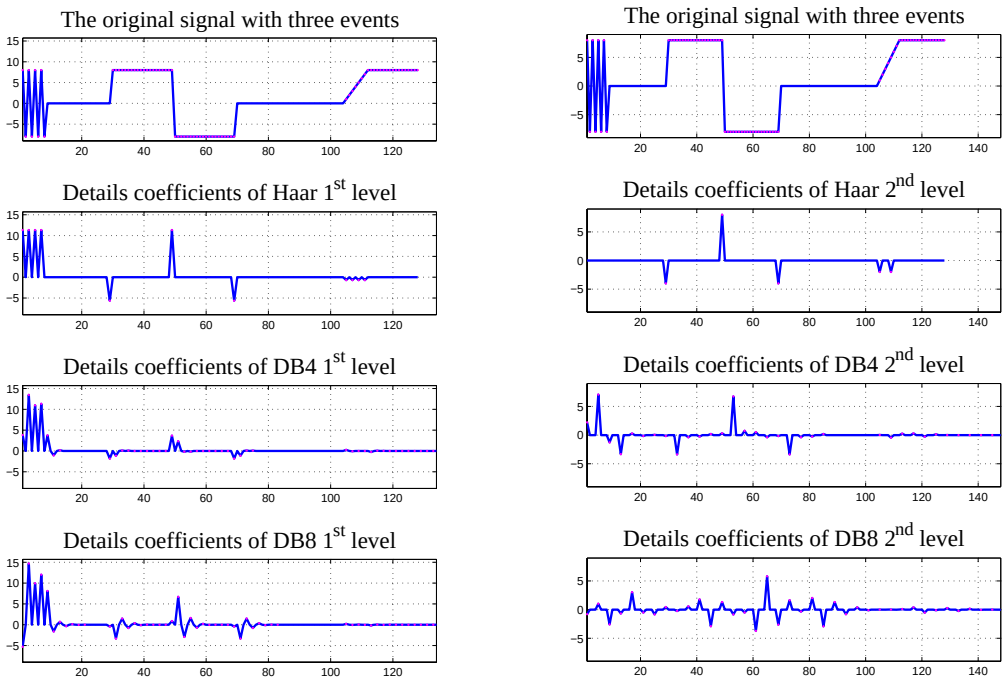

(a) (b)

Figure 2: Detail coefficients for a two level analysis by Haar, DB4, and DB8. Haar coefficients detect all the rapid changes in the 1^{st} level, while the detection of the wide edge lasts longer. Detection of events using the wavelets DB4 and DB8 comes shifted in position and distributed on a wider range.

2.2 Biorthogonal Wavelets

It is well known that bases that span a space do not have to be orthogonal. In order to gain greater flexibility in the construction of wavelet bases, the orthogonality condition is relaxed allowing semi-orthogonal, biorthogonal or non-orthogonal wavelet bases. Biorthogonal Wavelets are families of compactly supported symmetric wavelets. The symmetry of the filter coefficients is often desirable since it results in linear phase of the transfer function. In the biorthogonal case, rather than having one scaling and wavelet function, there are two scaling functions ϕ, $\widetilde{\phi}$, that may generate different multiresolution analysis, and accordingly two different wavelet functions ψ, $\widetilde{\psi}$. $\widetilde{\psi}$ is used in the analysis and ψ is used in the synthesis. In addition, the scaling functions ϕ, $\widetilde{\phi}$ and the wavelet functions ψ, $\widetilde{\psi}$ are related by duality in the following sense:

$$\int \psi_{j,k}(x)\widetilde{\psi}_{\acute{j},\acute{k}}(x)dx = 0 \tag{1}$$

as soon as $j \neq \acute{j}$ or $k \neq \acute{k}$ and even.

$$\int \phi_{0,k}(x)\widetilde{\phi}_{0,\acute{k}}(x)dx = 0 \tag{2}$$

as soon as $k \neq \acute{k}$.

A theorem by Cohen, Daubechies and Fauveau [1] gives sufficient conditions for building biorthogonal wavelets. The separation of analysis and synthesis is such that the useful properties for analysis (e.g., oscillations, zero moments) can be concentrated on the $\widetilde{\psi}$ function. The interesting property for synthesis (regularity) which is assigned to the ψ function has proven to be very useful.

The dual scaling and wavelet functions have the following properties:

1. They are zero outside of a segment.
2. The calculation algorithms are maintained, and thus very simple.
3. The associated filters are symmetrical.
4. The functions used in the calculations are easier to build numerically than those used in the Daubechies wavelets.

In this work biorthogonal B-spline wavelets were selected. B-splines are symmetrical, bell-shaped, piece-wise polynomial functions with good local properties. They were originally introduced by Chui and Wang [5, 4] as wavelet and scaling functions in multiresolution expansions. The B-spline wavelets have the following desirable properties: compact support, smoothness, symmetry, good localization, a simple analytical form in the spatial-frequency domain, and efficient implementation. They form a simple set of scaling functions satisfying the dilation equation with binomial filter coefficients. The biorthogonal wavelet functions Bior1.3 and Bior2.2 are illustrated in Fig. 3.

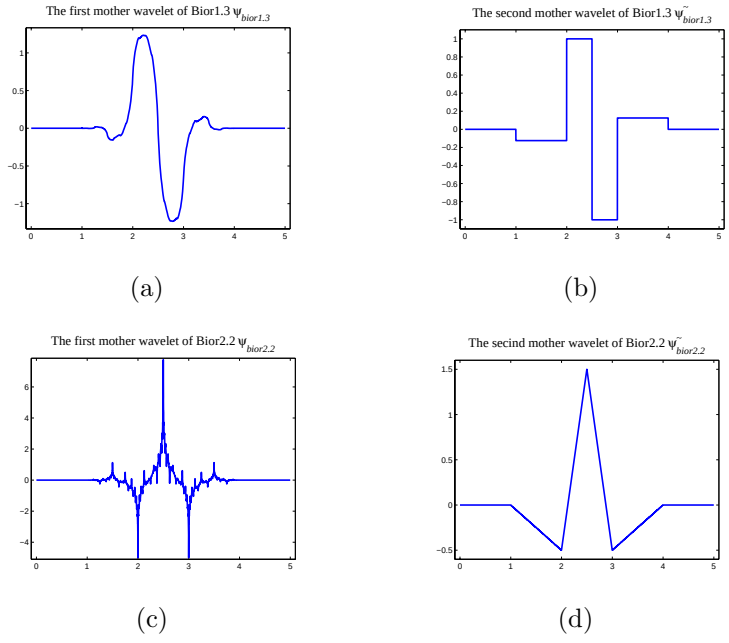

Figure 3: Biorthogonal wavelets Bior 1.3 and Bior 2.2.

It is convenient to name the biorthogonal wavelets as BiorNr.Nd, where Nr is the number of the order of the wavelet or the scaling functions used for reconstruction, while Nd is the order of the functions used for decomposition. The support width of the reconstruction and decomposition functions is $2Nr+1$ and $2Nd+1$, respectively. The length of the associated filters is $\mathsf{max}(2Nr, 2Nd) + 2$. However, the effective length of the filters associated with the wavelet functions $\psi_{Bior1.3}$ and $\widetilde{\psi}_{Bior1.3}$ and

$\psi_{Bior2.2}$ and $\widetilde{\psi}_{Bior2.2}$ is 2 and 3, respectively, and the effective length of the filters associated with the scaling functions $\phi_{Bior1.3}$ and $\widetilde{\phi}_{Bior1.3}$ and $\phi_{Bior2.2}$ and $\widetilde{\phi}_{Bior2.2}$ is 6 and 5, respectively.
Similar to the Daubechies wavelets, the analysis by the biorthogonal wavelets is done with some overlapping based on the effective length of the filters, except for Bior1.1, since it is the Haar wavelet.

2.3 3D Wavelet Transform

Multidimensional wavelet transform can be decomposed into a tensor product of orthogonal subspaces. Consequently, the 3D scaling function and the 3D wavelet functions can each be expressed as a product of three one-dimensional functions. The analysis is carried out along the $x-$, $y-$, and $z-$dimension of the volumetric data. Eight coefficients result from the one level analysis. One coefficient represents a volume approximation of the input data. The information which is missed in the approximation is distributed in the other 7 volume detail coefficients. Fig. 4 shows a one level 3D analysis done as three stand-alone 1D transforms.

The 3D dyadic scaling function ϕ and wavelet functions $\psi^i, i = 1, 2, ..7$, can be expressed as follows:

$$\phi_{j,\{k,l,m\}}(x,y,z) = 2^{\frac{3j}{2}}\phi(x-2^{-j}k)\phi(y-2^{-j}l)\phi(z-2^{-j}m) \tag{3}$$
$$\psi^1_{j,\{k,l,m\}}(x,y,z) = 2^{\frac{3j}{2}}\psi(x-2^{-j}k)\phi(y-2^{-j}l)\phi(z-2^{-j}m) \tag{4}$$
$$\psi^2_{j,\{k,l,m\}}(x,y,z) = 2^{\frac{3j}{2}}\phi(x-2^{-j}k)\psi(y-2^{-j}l)\phi(z-2^{-j}m) \tag{5}$$
$$\psi^3_{j,\{k,l,m\}}(x,y,z) = 2^{\frac{3j}{2}}\psi(x-2^{-j}k)\psi(y-2^{-j}l)\phi(z-2^{-j}m) \tag{6}$$
$$\psi^4_{j,\{k,l,m\}}(x,y,z) = 2^{\frac{3j}{2}}\phi(x-2^{-j}k)\phi(y-2^{-j}l)\psi(z-2^{-j}m) \tag{7}$$
$$\psi^5_{j,\{k,l,m\}}(x,y,z) = 2^{\frac{3j}{2}}\psi(x-2^{-j}k)\phi(y-2^{-j}l)\psi(z-2^{-j}m) \tag{8}$$
$$\psi^6_{j,\{k,l,m\}}(x,y,z) = 2^{\frac{3j}{2}}\phi(x-2^{-j}k)\psi(y-2^{-j}l)\psi(z-2^{-j}m) \tag{9}$$
$$\psi^7_{j,\{k,l,m\}}(x,y,z) = 2^{\frac{3j}{2}}\psi(x-2^{-j}k)\psi(y-2^{-j}l)\psi(z-2^{-j}m) \tag{10}$$
$$\tag{11}$$

Using Eqs. 3 to 10 the 3D analysis gives the following 8 subbands:

$$\begin{aligned} A_{j,\{k,l,m\}} &= \langle f(x,y,z),\ \phi_{j,\{k,l,m\}}(x,y,z)\rangle, \\ D^i_{j,\{k,l,m\}} &= \langle f(x,y,z),\ \psi^i_{j,\{k,l,m\}}(x,y,z)\rangle \\ & \qquad\qquad j \in \mathbb{Z}, \forall\{k,l,m\} \in \mathbb{Z}^3, \\ & \qquad\qquad i = 1, ..7 \end{aligned} \tag{12}$$

In Eq. 12 A_j is the low-pass subband at resolution level j and D^i_j is the high-pass subband i at resolution level j. For the fast 3D wavelet analysis only the low-pass subbands $A_{j,\{k,l,m\}}, j \in \mathbb{Z}, \{k,l,m\} \in \mathbb{Z}^3$ are used for further decomposition at lower

resolution levels. Therefore, it requires only $\mathcal{O}(n)$ computations [8]. The subband A is generated applying the scaling function ϕ to all the three dimensions of the data. So it represents the approximation in all axes. It can be used to replace the original data if no relevant changes occur. The subbands D^1, D^3, D^5, and D^7 are the result of applying the wavelet function ψ on the x-axis. So all of them contain information about the possible changes along the x-axis. Therefore, information about vertical edges can be easily obtained from such subbands. The subbands D^2, D^3, D^6, and D^7 and the subbands D^4, D^5, D^6, and D^7 can be explained in the same way as gradient information along the y-axis and z-axis, respectively. If the z-axis represents the time dimension, then the differences can be interpreted as a temporal change of illumination. Because movement means a change in spatial domains that follows the temporal change we think that the movement should be represented with the subband D^7.

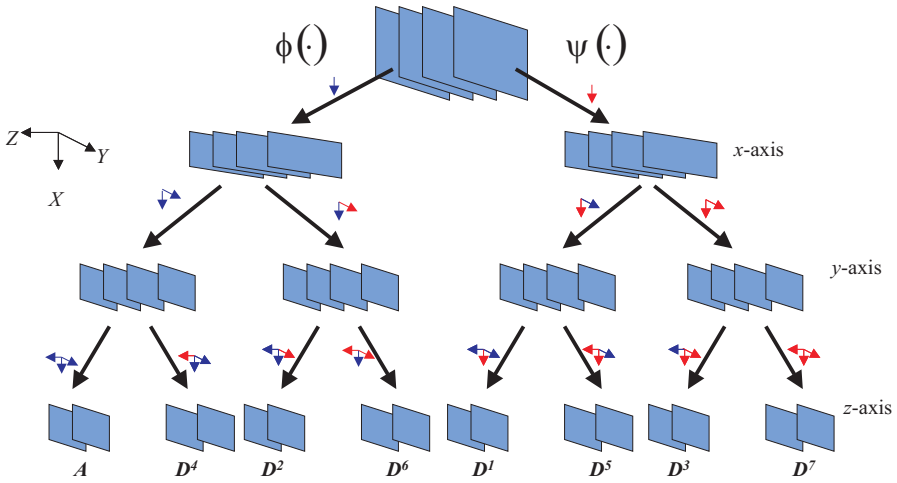

Figure 4: 3D Wavelet analysis as three one-dimensional transforms.

2.4 The 3D Wavelet-based Algorithm

In [15] a 3D wavelet-based algorithm for the detection of moving objects in a traffic surveillance video was proposed. The 3D algorithm has the advantage of considering the relevant spatial as well as temporal information of the movement. A movement in time sequence images is a three-dimensional change, two spatial dimensions and the time. Under this assumption, the detection of the moving objects is the answer to the question where and when there is a change in the local and temporal information.

The algorithm benefits from the multiresolution characteristics of the wavelet analysis. The analysis of an image sequence is done in different resolution levels. This speeds up the processing and improves the performance of the segmentation. In recent years multiresolution representation of images has got significant attention. But it has not been widely used for segmentation of time sequence images.

Moving object detection is performed by creating a mask from a group of frames which represents the regions of interest (ROI), where the moving objects supposed to be. The number of frames in a group depends on the level of the wavelet analysis. The proposed algorithm consists of three parts as shown in Fig. 5. It allows to derive a motion-based segmentation for any frame of the scene. In the first part, the 3D wavelet transform is used for the segmentation of the image sequence and produces a primary extraction of the ROI. The second part is a conventional procedure to improve the segmentation and to provide binary masks for the ROI. The final part

is a projection of the created masks onto the original images to extract the ROI in the original resolution. The first part is the only part that is affected by the choice of the wavelet function, therefore this is the only part described here.

The first and main part of the algorithm is the analysis of the input image sequence by the 3D wavelet transform. The input sequence is divided into groups of frames based on the analysis level. For the first level of the analysis only two frames are analyzed at once. For further levels the number of frames is equal to 2^j, where j is the analysis level. As already shown in Fig. 4, the results of the 3D wavelet transform are eight subbands, but only the subbands D^4 and D^7 are used for further processing. In general, the detail subbands have low intensity values. The subband D^4 shows relative high intensity values where events have occurred in time, while the subband D^7 shows events in all three dimensions. The subband D^7 represents a great part of the motion information in changes of the spatial and temporal domains. But its results show only the borders of the moving objects. It has been found that combining D^7 with other subbands improves the results. The combination with the subband D^4 has been found to give the best results because it represents the change between the approximations of successive frames. It shows the area where the movement occurs clearly. However, any changes in the pixel intensity between the processed frames also appear around the moving region so that its results are very noisy and cannot be used alone to extract the region of motion. That is why a simple average is used for the combination with the subband D^7.

The output of this step is a sequence of images with low intensities. The images have their highest intensity values where the movements are occurring and values near to zero otherwise. This step can be considered as a primary segmentation step that needs enhancements.

3 Simulation Results

To investigate the algorithm for the extraction of ROI many data sets were used and evaluated manually by a human operator. More statistical results and discussion about the accuracy of the segmentation in comparison with other methods are given in [15, 17].

In this paper the main objective is to compare the different wavelet types for the proposed application. Simulation results from four data sets are presented. All the data sets were captured using a stationary video camera. A summarized description of the data sets is shown in Table 1. The data sets can be categorized into two groups depending on the scene and the complexity of the movements. The first category, including set1 and set2, represents a simple scene of a front view with small camera observation angle to a street, where only a few cars are passing through. The second category, including set3 and set4, represents a complex scene of a wide view of a cross, where almost all types of moving traffic objects are present. Fig. 6 shows examples for both scenes.

For this study, a software program has been developed to enable a flexible experiment environment. The user is able to define the data set by giving the prefix name of the images and specifying the number of images and the starting serial number. It is assumed that all the images have the same prefix name and differ only by a postfix serial number. If the images are coloured, the tool converts them automatically into grey level images. All the wavelets available in the MATLAB

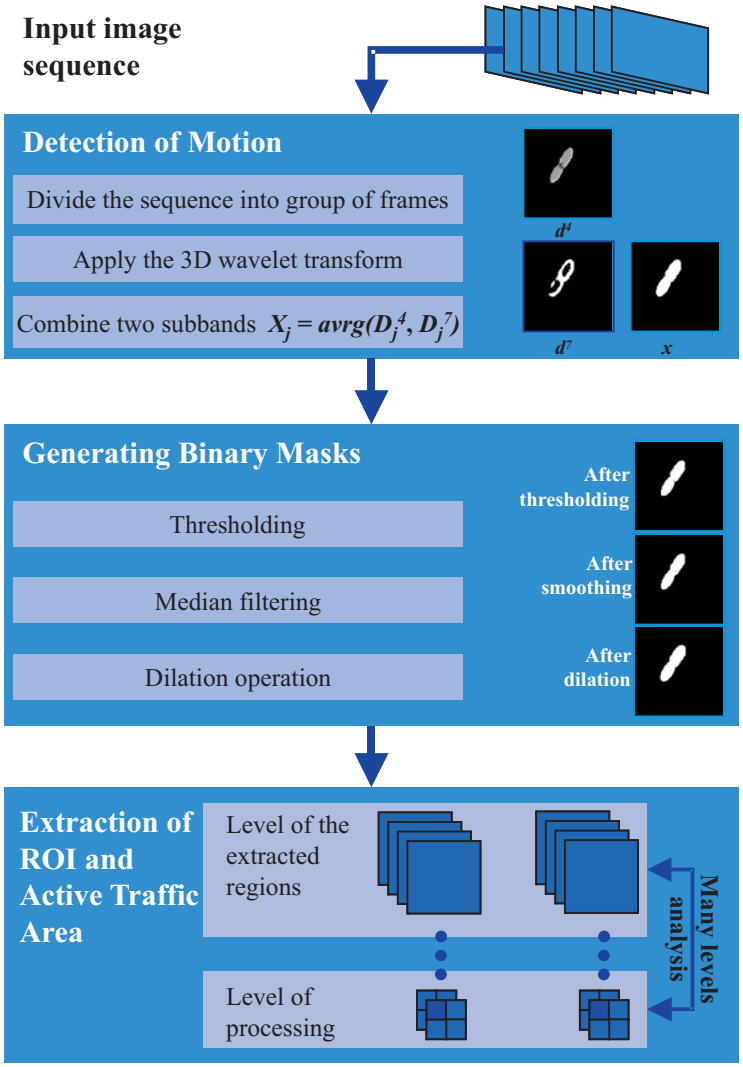

Figure 5: Block diagram of the 3D wavelet-based segmentation algorithm.

wavelet toolbox can be chosen by the user to perform the analysis for any given number of levels. The user can control the segmentation enhancement steps. He can choose different thresholding methods and decide which of the smoothing and dilation operations shall be performed and which filter setting should be chosen. The main feature of this program is that its commands can be put together and further modified to build the core of a toolbox for moving object detection in future work.

Output of the algorithm is a sequence of images showing the extracted ROI in the original resolution of the input images. For statistics and better presentations the ROIs are represented by their smallest bounding boxes. Generally, very small regions were neglected and considered as noise. The error is measured as false alarm rate and missed object rate. The false alarm rate is the ratio of the boxes that contain no objects relative to the total number of bounding boxes. The missed object rate is computed as the ratio of objects that are not contained in any box relative to the total number of moving objects. For the first data set two levels of wavelet analysis were applied because of its size, while for the other data sets three levels of analysis were applied. Tables 2 and 3 show the results of each data set at the different levels using different wavelets in terms of false alarms and missing objects rates.

(a) (b)

Figure 6: Examples of the used data sets for testing and evaluating the image sequence segmentation algorithms. (a) Example of the *Adlershof* data sets. (b) Example of the *Danziger* data sets.

Table 1: Description of the data sets used for the evaluation of the video segmentation algorithms.

Set No.	Prefix name	Seq. size	Frame/ second	Frames size	Image type	No. of objects
1	Adlershof1	12	25	288×352	Jpeg	13
2	Adlershof2	16	25	288×352	Jpeg	11
3	Danziger6	64	6	480×340	Bitmap	458
4	Danziger7	32	3	480×340	Bitmap	229

Figs. 7 and 8 show examples of an extracted ROI using different wavelets. Generally, the areas of the ROI become larger than the moving objects as the analysis level increases. This is due to the decrease in the temporal resolution. Fig. 7 shows samples of the results of the first data set. The results show comparable detection of the objects applying the Haar and biorthogonal wavelet, while for the DB4 wavelet the accuracy of the algorithm is affected by the irregularity of the wavelets in terms of increased false alarm rates. The results of the second data set emphasize the effect of the wavelet features on the visual results, such as the function length, the symmetry and the irregularity. Fig. 8(a) shows an image composed of two frames and a boundary for the ROI done by hand. Fig. 8(b) shows that the detection by the Haar wavelet is localized. However, there are sharp transitions between the ROI and the background. In many applications a smooth transition is highly desired. In Fig. 8(c) the results of the biorthogonal wavelets show that the detected object is centred in the ROI, which can be explained by the biorthogonal wavelet symmetry properties. In contrast, the results of the Daubechies wavelet as shown in Fig. 8(d) are shifted to the left. Thus, we have a too early detection of moving objects due to the wavelet function length of DB4 and its irregularity. The third and the fourth data sets are used mainly for the statistical results since they represent long observations with many moving objects. The results of both the Haar and biorthogonal wavelets are comparable and superior to those obtained by the DB4. However, as the level of analysis increases the rate of missed objects decreases for all the wavelet types.

Table 2: False alarm rate for the different data sets.

		Haar	DB4	DB8	Bior1.3	Bior2.2
Set 1	Level 1	14%	46%	41%	19%	19%
	2	25%	69%	46%	35%	35%
Set 2	Level 1	8%	45%	50%	8%	8%
	2	31%	67%	68%	31%	31%
	3	31%	75%	66%	31%	31%
Set 3	Level 1	0%	10%	13%	9%	4%
	2	5%	20%	18%	23%	13%
	3	4%	31%	31%	13%	15%
Set 4	Level 1	3%	19%	26%	12%	6%
	2	5%	40%	37%	26%	31%
	3	1%	25%	17%	25%	31%

Table 3: Missed object rates for the different data sets.

		Haar	DB4	DB8	Bior1.3	Bior2.2
Set 1	Level 1	0%	0%	0%	0%	0%
	2	0%	15%	0%	0%	0%
Set 2	Level 1	0%	0%	0%	0%	0%
	2	0%	0%	0%	0%	0%
	3	0%	27%	0%	0%	0%
Set 3	Level 1	11%	13%	23%	9%	18%
	2	2%	6%	12%	8%	8%
	3	0%	9%	10%	3%	4%
Set 4	Level 1	3%	8%	16%	12%	13%
	2	1%	2%	4%	7%	7%
	3	0%	3%	13%	0%	7%

4 Discussion and Conclusion

Alg. Summery

The 3D wavelet based algorithm is reliable to detect objects entering a scene. The proposed algorithm tends to detect the objects in groups, especially when they move close together. This group detection depends on the number of frames that are processed at a time and on the level of the analysis. The results illustrate examples of extracted ROI of all levels. A main feature of the multiresolution algorithm is that the processing is done in a lower spatial resolution than that of the input images. Therefore the computational complexity is reduced considerably. The 3D wavelet transform utilizes temporal information of the motion as well as spatial information. The information contained in the image sequences can be a subject for approximation and differencing. Such processing has many advantages in video transmission between different components of the monitoring system like camera, processing unit, and terminals for further decision making.

Haar better for ROI detection

The algorithm is applied to the different image sequences using Daubechies and biorthogonal wavelets to study the effect of the properties of the wavelet functions on the analysis. The results show that the Haar wavelet provides good detection of the moving object because of its localization property.

The problem of long wavelets

The longer filters associated with the other wavelets lead to overlapping in the analysis, which consequently makes the sharp edges be detected as wide events. Since the localization of the event detection is the main concern the overlapping analysis has to be considered as a disadvantage. It affects the segmentation by producing enlarged ROIs.

Bior is better than DB because..

The symmetry property of biorthogonal wavelet is also exploited for the detection. It improves the rate of missed objects as they were centred in the extracted ROI. The results obtained from the DB4 wavelets are inferior compared to both previous wavelets, because the irregularity of the wavelet affects the detection of moving

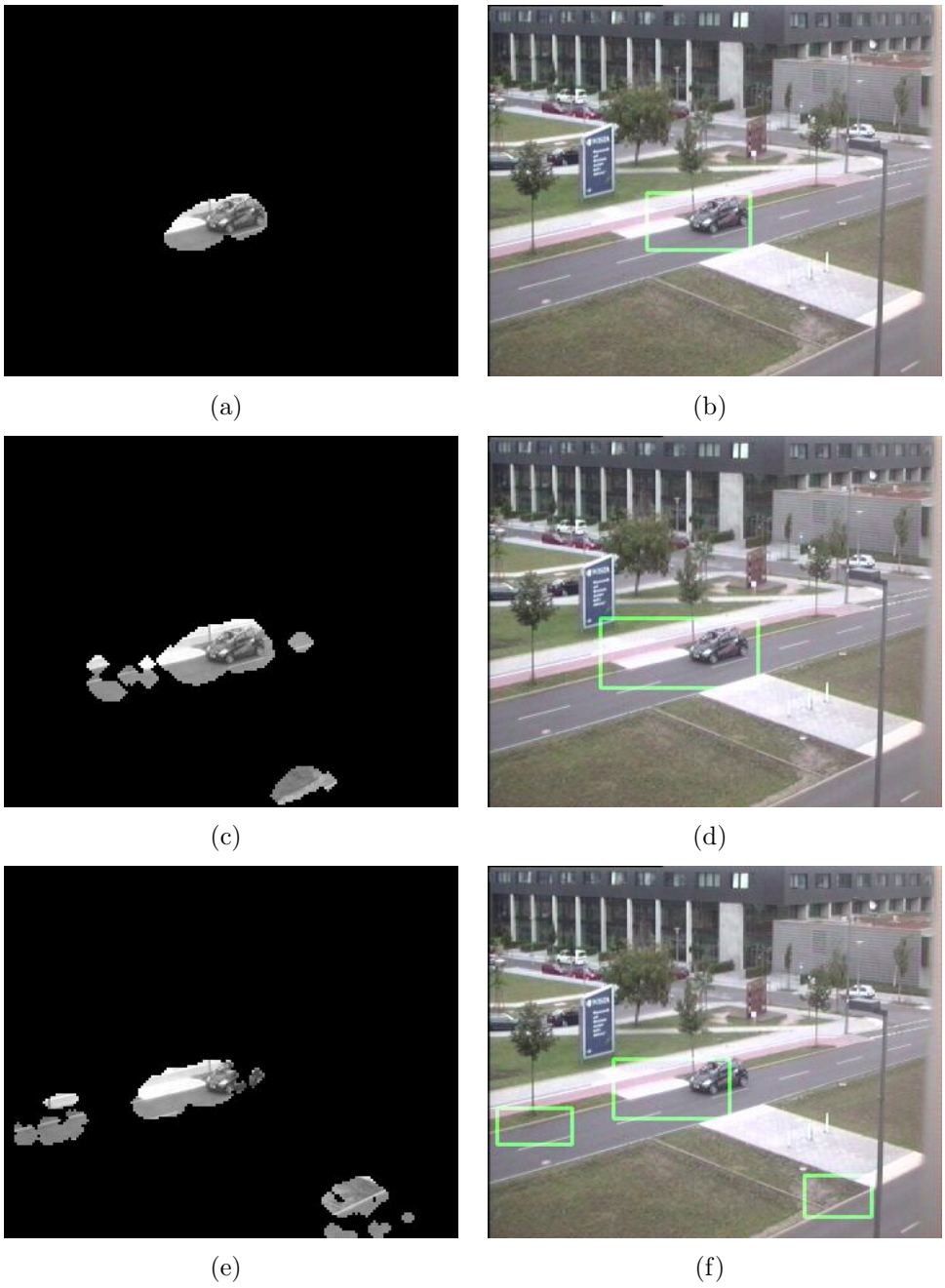

(a) (b) (c) (d) (e) (f)

Figure 7: Extraction of ROI and the corresponding bounding boxes for the data set *Adlershof1*. (a) and (b) Haar wavelet. (c) and (d) Bior1.3. (d) and (f) DB4.

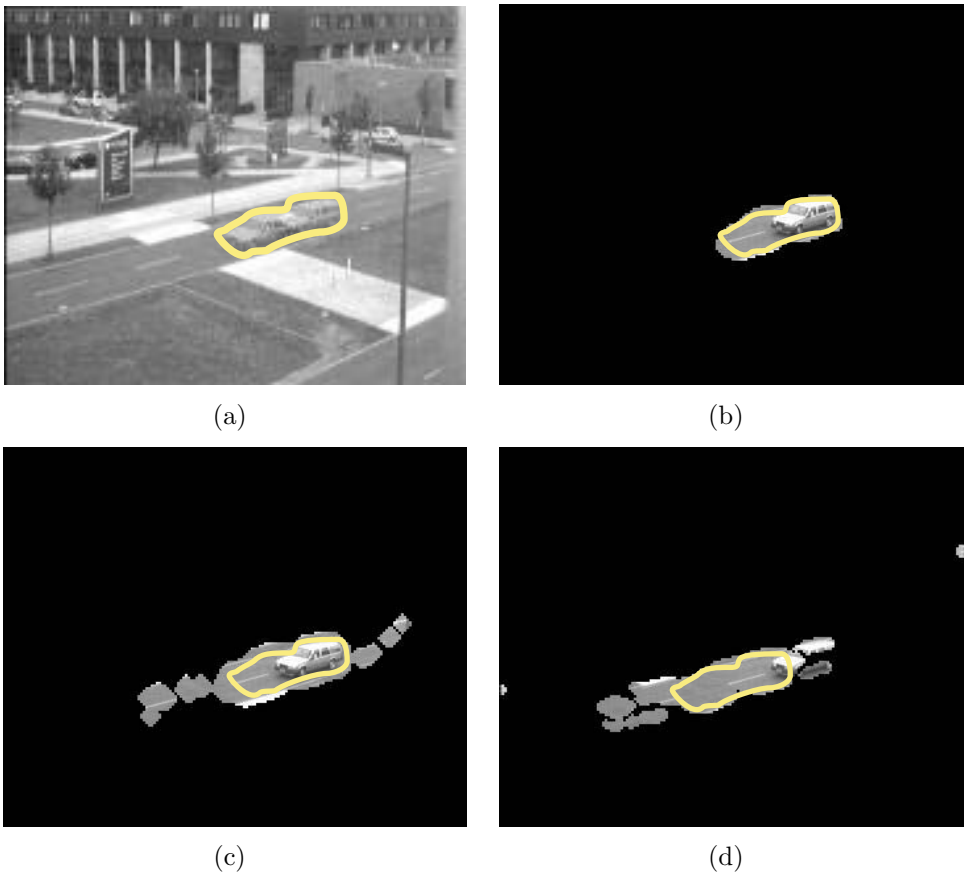

(a) (b)

(c) (d)

Figure 8: Localization of the extracted ROI. (a) Motion in two successive frames from the data set *Adlershof2*. The ROI using (b) Haar wavelet. (c) Bior1.3. (d) DB4.

objects to a far extent. "Too" many pixels from the right areas to the pixels that are processed currently are taken into consideration by the analysis. This leads to a misestimation of these parts. As a result the extracted regions become bigger than the moving objects and are shifted to the left. This is clearly seen by the results of the data set *Adlershof2* because the objects are moving from the right end of the scene to the left end.

Complexity

Moreover, the complexity of the computation increases as the length of the filters increases.

Overlapping is good 4 comp.

In other applications, such as lossy video compression, the overlapping analysis can be counted as an advantage. The information content in a certain segment of the video will be copied in various coefficients. Discarding some of the coefficients for the purpose of compression will not lead to a loss of information, since they are represented somewhere else. Thus, as the overlapping increases, high compression rates with better reconstruction of the video can be achieved.

HW Implemenattion

Due to the simplicity of the Haar wavelets, parts of the algorithm were implemented on specialized hardware which can be included in a camera [16].

References

[1] J.-C. Feauveau A. Cohen, Ingrid Daubechies. Biorthogonal bases of compactly supported wavelets. *Communications on Pure and Applied Mathematics*, 45(5):485–560, 1992.

[2] M. Bramberger, J. Brunner, B. Rinner, and H. Schwabach. Real time video analysis on a smart camera for traffic surveillance. In *10th IEEE Real-Time and Imbedded Technology and Applications Symposium (RTAS 04)*. IEEE Computer Society, 2004.

[3] Evelyn Brannock and Michael Weeks. Edge detection using wavelets. In *ACM-SE 44: Proceedings of the 44th Annual Southeast Regional Conference*, pages 649–654, New York, NY, USA, 2006. ACM.

[4] Andrea Cavallaro. *From Visual Information to Knowledge*. PhD thesis, Lausanne, Switzerland, 2002.

[5] Charles K. Chui and Jian-Zhong Wang. On compactly supported spline wavelets and a duality principle. *Transactions of the American Mathematical Society*, 330(2):903–915, 1992.

[6] R.T. Collins, A.J. Lipton, T. Kanade, H. Fujiyoshi, D. Duggins, Y. Tsin, D. Tolliver, N. Enomoto, O. Hasegawa, P. Burt, and L. Wixson. A system for video surveillance and monitoring. Technical Report CMURI-TR-00-12, Carnegie Mellon University, 2000.

[7] Ingrid Daubechies. *Ten Lectures on Wavelets*. Society for Industrial and Applied Mathematics, 1992.

[8] Anca Dima. *Computer Aided Image Segmentation and Graph Construction of Nerve Cells from 3D Confocal Microscopy Scan*. PhD thesis, Technical University Berlin, Department of Neuronal Information Processing, 2002.

[9] P.J. Figueroa, N.J. Leite, and R. Barros. Background recovering in outdoor image sequences: An example of soccer players segmentation. *Image and Vision Computing*, 24(4):363–374, April 2006.

[10] Ashish Khare and Uma Shanker Tiwary. Soft-thresholding for denoising of medical images - a multiresolution approach. *International Journal of Wavelets, Multiresolution and Information Processing*, 3(4):477–496, April 2005.

[11] Z.W. Kim and J. Malik. Fast vehicle detection with probabilistic feature grouping and its application to vehicle tracking. In *IEEE International Conference on Computer Vision*. IEEE Computer Society, 2003.

[12] Stéphane G. Mallat. A theory for multiresolution signal decomposition, the wavelet representation. *IEEE Transaction on Pattern Analysis and Machine Intelligence*, 2(7):674–693, 1989.

[13] Y. Park. Shape-resolving local thresholding for object detection. *Pattern Recognition Letters*, 22:883–890, 2001.

[14] Saleem, Touqir, and Siddiqui. Novel edge detection. In *ITNG*, pages 175–180, Los Alamitos, CA, USA, 2007. IEEE Computer Society.

[15] Mohammed A-Megeed Salem. Application of the 3D wavelet transform on lane extraction on traffic monitoring images. In *Wavelets and Applications, wavE2006*, Lausanne, Switzerland, July 10-14 2006.

[16] Mohammed A-Megeed Salem, Markus Appel, Frank Winkler, and Beate Meffert. FPGA-based smart camera for 3D wavelet-based image segmentation. In *2nd ACM/IEEE International Conference on Distributed Smart Cameras (ICDSC-08)*, Stanford, California, USA, September 7-11 2008. Stanford University.

[17] Mohammed A-Megeed Salem and Beate Meffert. A comparison between 2D and 3D wavelet-based segmentation for traffic monitoring systems. In *3rd International Conference on Intelligent Computing and Information Systems*, Cairo, Egypt, March 15-18 2007.

[18] B. Ugur Töreyin, A. Enis Cetin, Anil Aksay, and M. Bilgay Akhan. Moving object detection in wavelet compressed video. *Signal Processing: Image Communication*, 20:255–264, March 2005.

[19] Y. Won, J. Nam, and B.-H. Lee. Image pattern recognition in natural environment using morphological feature extraction. In *SSPR & SPR 2000; F.J. Ferri (Ed.)*, pages 806–815, Berlin, 2001. Springer.

[20] Q. Zang and R. Klette. Object classification and tracking in video surveillance. In *10th International Conference of Computer Analysis of Images and Patterns, CAIP*, volume 2756, pages 198–205, Groningen, The Netherlands, August 25-27 2003. Springer Berlin / Heidelberg.